

Non-perturbative cathodoluminescence microscopy of beam-sensitive materials

Malcolm Bogroff*,¹ Gabriel Cowley*,¹ Ariel Nicastro*,¹ David Levy,¹ Yueh-Chun Wu,¹ Nannan Mao,² Tilo H. Yang,² Tianyi Zhang,² Jing Kong,² Rama Vasudevan,³ Kyle P. Kelley,³ and Benjamin J. Lawrie^{1,3}

¹*Materials Science and Technology Division, Oak Ridge National Laboratory, 1 Bethel Valley Rd, Oak Ridge, TN 37831*

²*Electrical Engineering and Computer Science Department, Massachusetts Institute of Technology, 77 Massachusetts Ave. Cambridge, MA 02139*

³*Center for Nanophase Materials Sciences, Oak Ridge National Laboratory, 1 Bethel Valley Rd, Oak Ridge, TN 37831*

(Dated: 17 December 2024)

Cathodoluminescence microscopy is now a well-established and powerful tool for probing the photonic properties of nanoscale materials, but in many cases, nanophotonic materials are easily damaged by the electron-beam doses necessary to achieve reasonable cathodoluminescence signal-to-noise ratios. Two-dimensional materials have proven particularly susceptible to beam-induced modifications, yielding both obstacles to high spatial-resolution measurement and opportunities for beam-induced patterning of quantum photonic systems. Here pan-sharpening techniques are applied to cathodoluminescence microscopy in order to address these challenges and experimentally demonstrate the promise of pan-sharpening for minimally-perturbative high-spatial-resolution spectrum imaging of beam-sensitive materials.^a

I. INTRODUCTION

Color centers and localized excitons in two-dimensional (2D) materials have emerged as a promising resource for quantum networking and quantum sensing in recent years^{1–4} because of the potential for atomic scale control over the defect environment^{5,6}, compatibility with integrated photonic circuits^{3,4,7,8}, and the potential for manipulation of emitter photophysics with engineered strain environments^{9–13} and electrical gating^{14–16}. Unfortunately, many reports in the literature focus on ‘hero’ emitters that are selected after exhaustive searches of many lower quality emitters. Attempts to locate and pattern individual single photon emitters with desirable brightness, purity, and indistinguishability often result in the observation of multiple emitters within a single diffraction-limited spot or in the emergence of coupled electronic transitions with unwanted photochromic effects^{17,18}. The ability to manipulate and measure the quantum states associated with these color centers relies heavily on our understanding of how nanoscale heterogeneities affect their photophysical behavior. Therefore, advanced nanoscale probes that can accurately assess these effects while allowing for in situ modification are crucial to the development of color centers for practical quantum technologies.

Cathodoluminescence (CL) microscopies have emerged as a powerful nanoscale probe of quantum nanophotonic systems^{10,13,19–23}. The converged electron-beam probe of-

fers a nanometer-scale excitation, and far-field collection of CL enables high sensitivity measurements of emitter energetics and dynamics across a wide variety of energy- and time-scales. However, the electron-beam probe has also emerged as a resource for beam-induced modification of 2D materials^{20,24–26}. Indeed, many monolayer transition metal dichalcogenides only exhibit measurable CL signals when they are encapsulated by hBN^{21,22}, an effect that may result from beam-induced damage to beam-sensitive materials. While clear examples exist in the literature using the electron beam to either probe or manipulate color centers in 2D materials, the necessary electron-beam dose to measure emitter photophysics is in many cases also sufficient to substantially modify the defect environment in that material. Thus, identifying new minimally-perturbative approaches to CL microscopy capable of probing the color center environment without modifying it — while allowing for intentional in situ modification at higher electron-beam doses — is critical to improved understanding and control of 2D quantum photonic systems.

Pan-sharpening (PS) methods may offer a minimally perturbative approach to CL microscopy by combining separate high-spatial-resolution and high-spectral-resolution images in order to generate a composite image with both high spatial and spectral resolution. First used in satellite imaging^{27,28}, PS methods have now emerged as powerful tools for multidimensional imaging in a wide variety of use cases. In nanoscience, PS has been applied to electron energy loss spectroscopy²⁹, scanning probe microscopy³⁰, and secondary ion mass spectrometry³¹, though PS-CL has not yet been explored despite the substantial benefit associated with minimizing beam-induced damage through undersampling of hyperspectral CL images. Most PS algorithms rely on either (i) the substitution of spectral components from a hyperspectral dataset with a high spatial resolution panchromatic image or (ii) a multiresolution analysis approach based on injection of spatial details from the panchromatic image into resampled hyperspectral bands³². Here, we focus on PS-CL performed

^aThis manuscript has been authored by UT-Battelle, LLC, under contract DE-AC05-00OR22725 with the US Department of Energy (DOE). The US government retains and the publisher, by accepting the article for publication, acknowledges that the US government retains a nonexclusive, paid-up, irrevocable, worldwide license to publish or reproduce the published form of this manuscript, or allow others to do so, for US government purposes. DOE will provide public access to these results of federally sponsored research in accordance with the DOE Public Access Plan (<http://energy.gov/downloads/doe-public-access-plan>).

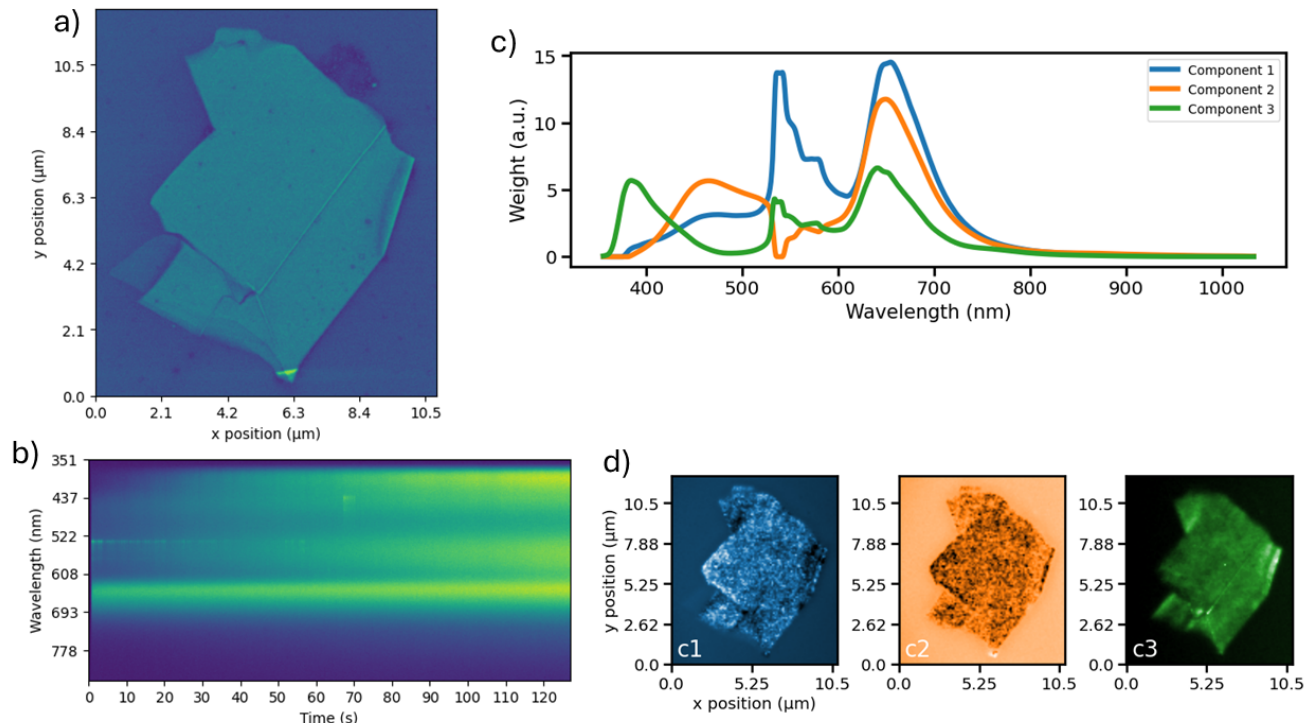


FIG. 1. (a) SEM image of an hBN flake with horizontal width of 10.5 microns. (b) Time-series CL spectra acquired at a single point on the hBN flake highlighting the beam-induced changes in the hBN CL spectrum as a function of increasing dose. (c) Spectral components and (d) intensity maps generated by non-negative matrix factorization of CL spectrum image acquired in conventional rastered CL spectrum imaging modality.

using the Brovey transform³³, an example of the former class of PS algorithms that uses multiplicative sharpening to spatially modulate spectral pixels³², and we examine the impact of this approach on CL imaging of color centers in 2D materials.

II. METHODS

Hexagonal boron nitride (hBN) is known to be relatively robust to electron-beam exposure, and it has been probed by conventional CL microscopy¹³, but there is also a growing literature describing electron-beam induced patterning of color centers in hBN^{20,24–26}. Thus, hBN offers a valuable platform for examining PS-CL techniques that could be crucial to probes of more environmentally sensitive materials like monolayer transition metal dichalcogenides and some classes of hybrid organic perovskite thin films. All data reported here is based on exfoliated hexagonal boron nitride (hBN) flakes transferred onto a 300 nm silicon dioxide (SiO₂) layer on a silicon substrate.

Cathodoluminescence data was acquired using a Delmic Sparc CL module with an FEI Quattro scanning electron microscope (SEM) operating with a beam energy of 5 kV and a beam current of 110 pA at room temperature and a chamber pressure of 1E-6 Torr. CL spectrum images were ac-

quired with an Andor Kymera spectrograph and an Andor Newton CCD with an acquisition time of 300 ms per spectrum. A pickoff mirror was used to direct the collected CL signal into a photomultiplier tube (PMT) for high-spatial resolution panchromatic CL imaging using a PMT integration time of 10 μs (yielding 30,000x reduced dose per pixel compared with spectrum imaging).

III. RESULTS

An SEM image of a prototypical hBN flake is illustrated in Fig. 1(a). While we were able to acquire moderately coarse spatial resolution CL spectrum images of hBN flakes with no apparent degradation (with pixel sizes of order 100 nm), improving spatial resolution while maintaining the beam energy and current along with a constant dwell time per pixel resulted in growing evidence of beam-induced modification of the hBN flake. This dose-dependent beam-induced modification is most easily visualized through time-series spectra acquired while the electron beam rapidly scanned 768x512 pixels across a 500 nm spot with a 100 ns/pixel electron dwell time. Note that acquiring time-series spectra with the electron beam focused on a single spot resulted in immeasurably fast changes in the CL spectra, so averaging across a 500 nm spot allowed us to reduce the effective dose/pixel during

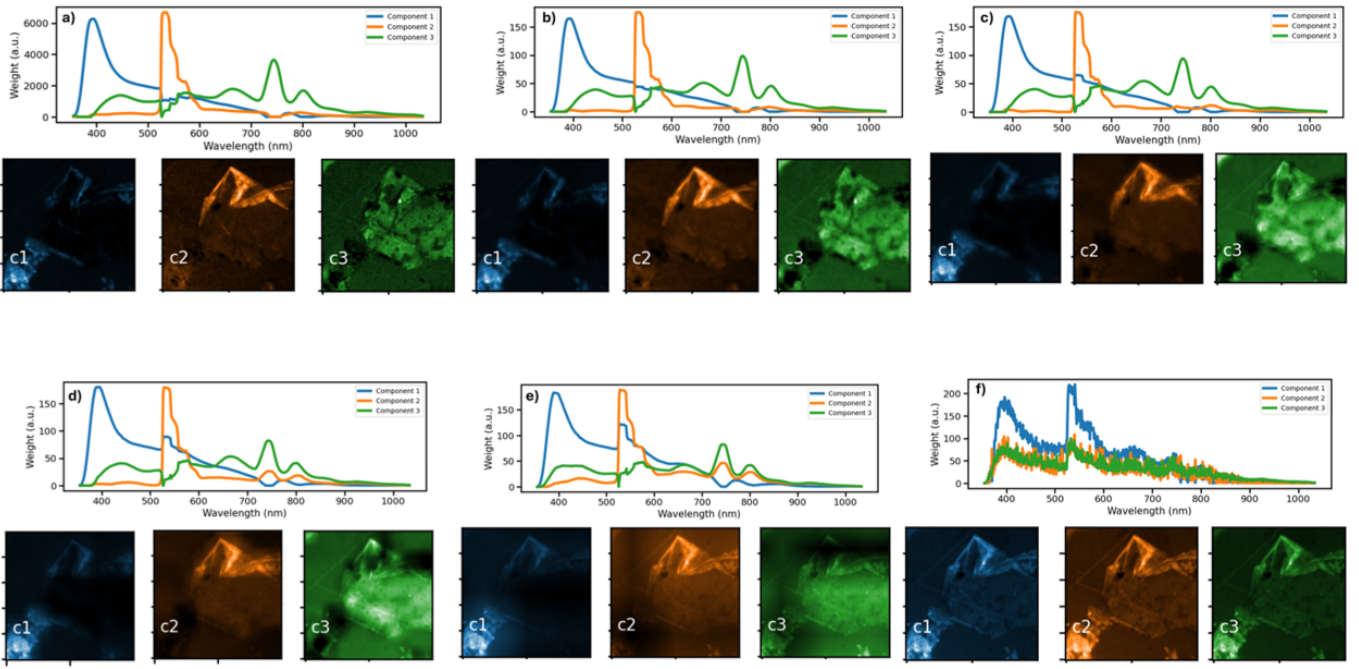


FIG. 2. Benchmark PS-CL results generated from a single CL hyperspectral image of an hBN flake with dimensions of $100 \times 100 \times 1024$ (horizontal, vertical, wavelength) pixels with a horizontal field of view of $30 \mu\text{m}$. A panchromatic image was generated from the spectrum image by summing along the wavelength axis while spectrum images with reduced spatial resolution were generated by binning spatial pixels together. The Brovey pan-sharpening algorithm was used to reconstruct a hyperspectral CL image from these datasets. NMF reconstructions of the pan-sharpened CL images are shown for data generated from the panchromatic image and (a) the complete $100 \times 100 \times 1024$ spectrum image, (b) a $50 \times 50 \times 1024$ spectrum image, (c) a $25 \times 25 \times 1024$ spectrum image, (d) a $12 \times 12 \times 1024$ spectrum image, (e) a $6 \times 6 \times 1024$ spectrum image, and (f) a $1 \times 1 \times 1024$ spectrum image.

time-series CL spectrum acquisition. A reduced CL spectrum acquisition time of 100 ms (approximately 2.5x the time required to scan 768×512 pixels) was used in order to monitor the time-dependent changes in CL spectra as a function of electron-beam dose.

Several features are immediately apparent in the time-series spectra shown in Fig. 1(b): A prominent CL band centered at a wavelength of 660 nm exhibits minimal change with increasing dose. On the other hand, a blue CL band near 408 nm grows monotonically with increasing dose, and the CL from a narrow linewidth color center near 548 nm disappears with increasing dose. These results highlight the importance of alternative SEM-CL acquisition modalities, especially for smaller pixel sizes where the increased electron-beam dose can result in rapid modification of the hBN color center photophysics. Additionally, it is difficult to interpret CL spectra acquired at a single point, as we expect some CL contribution from defect bands in the SiO_2 substrate.

Figures 1(c) and (d) illustrate a non-negative matrix factorization (NMF) decomposition of a CL spectrum image acquired across this flake using conventional raster scanning with a pixel size of 100 nm. For all NMF decompositions shown in this manuscript, reconstructions were attempted with varying numbers of components, and it was determined that three components were sufficient to provide a reasonable reconstruction of the raw data. The NMF decomposition shown in Fig. 1 immediately aids in the interpretation

of the single point CL spectra shown in Fig. 1(b): Component 3 is solely a result of the hBN flake, while Component 2 appears to be primarily a result of the SiO_2 substrate luminescence. Component 1, which features the narrow transition at 548 nm, appears to be primarily due to the hBN flake, though it includes some convolution with substrate luminescence.

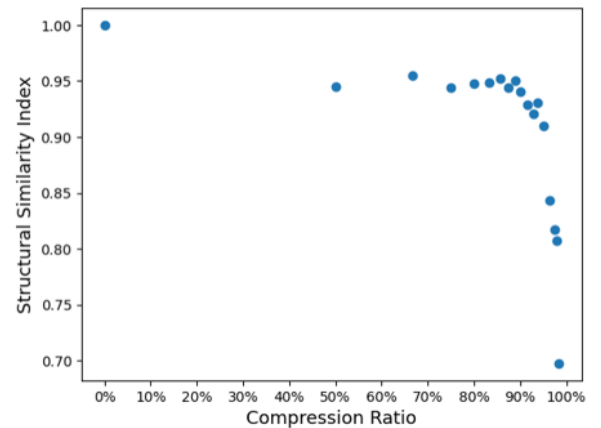


FIG. 3. Calculated structural similarity index as a function of compression ratio for the PS-CL data shown in Fig. 2. The compression ratio is calculated based on the compression of the hyperspectral data prior to pan sharpening.

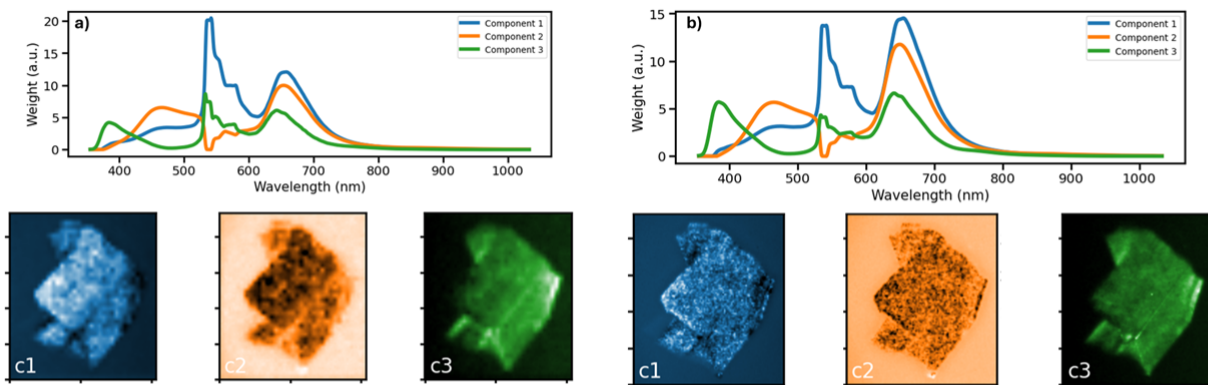


FIG. 4. Three component NMF reconstructions of hBN PS-CL images generated from (a) an 1168×1034 pixel panchromatic image and a 39×35 pixel hyperspectral image and (b) an 1168×1034 panchromatic image and a 117×105 pixel hyperspectral image. The horizontal field of view is $10.5 \mu\text{m}$.

cence. The narrow band color centers seen in Component 1 are reasonably densely distributed across the hBN flake. Unfortunately, it is hard to image these color centers with improved spatial resolution using conventional CL raster scanning because reducing pixel sizes while maintaining the field of view yields a combination of beam-induced damage and unacceptably long measurement times. However, PS-CL techniques offer a promising pathway to address this challenge.

The Brovey transform was identified as a PS algorithm well suited to our data, and it was benchmarked by generating high spatial resolution and high spectral resolution datasets from a single $100 \times 100 \times 1024$ (horizontal \times vertical \times wavelength) pixel hyperspectral CL image of a hBN flake (by separately binning all wavelengths together to create a 100×100 pixel panchromatic image and binning adjacent spatial pixels to create spectrum images with 1024 spectral pixels and between 1×1 and 50×50 spatial pixels). We then up-sampled the hyperspectral dataset to match its spatial resolution with that of the panchromatic image using the `resize` function in `skimage.transform` with linear splines. Each spatial pixel's spectrum in this new dataset is scaled to match the net intensity of the corresponding normalized panchromatic pixel's intensity. The pan-sharpened CL spectrum image then had dimensions of $100 \times 100 \times 1024$ and could be easily compared with the original spectrum image.

Three component NMF reconstructions of the PS-CL image with reduced dimensionalities are shown in Fig. 2. At first glance, very little information is lost in the PS-CL image as the hyperspectral image is collapsed from a $100 \times 100 \times 1024$ spectrum image (Fig. 2 (a)) to a $6 \times 6 \times 1024$ image (Fig. 2 (e)), though unsurprisingly, all three components of the PS-CL image generated from a $1 \times 1 \times 1024$ spectrum image (Fig. 2 (f)) look nearly identical to one another. The quality of the pan-sharpening algorithm can be calculated here with a structural similarity index (SSI) comparing the pan-sharpened image with the original $100 \times 100 \times 1024$ spectrum image. The SSI of each pan-sharpened image here was calculated using the `scikit-image` library. As shown in Fig. 3, applying the Brovey transform to the original $100 \times 100 \times 1024$ spectrum image results in a SSI of 1.0, and a $\text{SSI} > 0.9$ for compres-

sion ratios as high as 90%.

This baseline PS-CL data suggests that CL spectrum images can be acquired with substantially reduced electron-beam exposure by combining short-dwell-time panchromatic CL images acquired on a PMT with very low spatial resolution spectrum images. Further, rastering the electron-beam over each spectrum-image pixel during the comparably-slow spectrum acquisition time will distribute the electron-beam dose over a large area and minimize the risk of beam-induced damage.

With this understanding in hand, PS-CL images were reconstructed from raw hyperspectral and panchromatic CL datasets. Figure 4 illustrates three-component NMF reconstructions of PS-CL images of an hBN flake generated from an 1168×1034 panchromatic CL image (using $10 \mu\text{s}$ dwell time per pixel) and a 39×35 pixel spectrum image (Fig. 4(a)) and a 117×105 pixel spectrum image (Fig. 4(b)) (each using a 300 ms spectrum acquisition time per pixel). Both exhibit very similar spectral components, though the latter does exhibit higher-spatial-resolution intensity maps. Nonetheless, these results show the potential impact of pan-sharpening for CL microscopy with minimal beam-induced damage.

IV. CONCLUSION

The PS-CL results shown here suggest that hyperspectral CL measurements can be undersampled by 90% while maintaining at least 90% fidelity to the ground truth. Because hyperspectral and panchromatic datasets can be easily acquired concurrently (using a beamsplitter) or consecutively (using a pickoff mirror) with no change to the experimental alignment, the approach described here is easily adapted for a wide variety of CL microscopies of beam-sensitive materials. This approach is particularly critical for minimizing beam-induced damage in beam-sensitive materials like monolayer 2D materials and hybrid organic perovskite thin films, and for applications that require high spatial resolution and long spectrum acquisition times. The successful demonstration of PS-CL also unlocks new opportunities for high-dose electron-beam pat-

tering of single photon emitters with low dose PS-CL in situ characterization.

ACKNOWLEDGMENTS

This research was supported by the U. S. Department of Energy, Office of Science, Basic Energy Sciences, Materials Sciences and Engineering Division. CL microscopy and data analytics algorithms were supported by the Center for Nanophase Materials Sciences, which is a U.S. Department of Energy Office of Science User Facility. MB, GC, AN, and DL were supported by the U.S. Department of Energy, Office of Science, Office of Workforce Development for Teachers and Scientists (WDTS) under the Science Undergraduate Laboratory Internship program.

- ¹I. Aharonovich, D. Englund, and M. Toth, "Solid-state single-photon emitters," *Nature photonics* **10**, 631–641 (2016).
- ²M. Atatüre, D. Englund, N. Vamivakas, S.-Y. Lee, and J. Wrachtrup, "Material platforms for spin-based photonic quantum technologies," *Nature Reviews Materials* **3**, 38–51 (2018).
- ³X. Liu and M. C. Hersam, "2d materials for quantum information science," *Nature Reviews Materials* **4**, 669–684 (2019).
- ⁴M. Turunen, M. Brotons-Gisbert, Y. Dai, Y. Wang, E. Scerri, C. Bonato, K. D. Jöns, Z. Sun, and B. D. Gerardot, "Quantum photonics with layered 2d materials," *Nature Reviews Physics* **4**, 219–236 (2022).
- ⁵O. Dyck, S. Kim, E. Jimenez-Izal, A. N. Alexandrova, S. V. Kalinin, and S. Jesse, "Building structures atom by atom via electron beam manipulation," *Small* **14**, 1801771 (2018).
- ⁶O. Dyck, A. R. Lupini, and S. Jesse, "Atom-by-atom direct writing," *Nano Letters* **23**, 2339–2346 (2023).
- ⁷E. Pelucchi, G. Fagas, I. Aharonovich, D. Englund, E. Figueroa, Q. Gong, H. Hannes, J. Liu, C.-Y. Lu, N. Matsuda, *et al.*, "The potential and global outlook of integrated photonics for quantum technologies," *Nature Reviews Physics* **4**, 194–208 (2022).
- ⁸L. Spencer, J. Horder, S. Kim, M. Toth, and I. Aharonovich, "Monolithic integration of single quantum emitters in hbn bullseye cavities," *ACS Photonics* **10**, 4417–4424 (2023).
- ⁹W. Luo, A. A. Purezky, B. J. Lawrie, Q. Tan, H. Gao, Z. Chen, A. V. Sergienko, A. K. Swan, L. Liang, and X. Ling, "Deterministic localization of strain-induced single-photon emitters in multilayer gas," *Acs Photonics* **10**, 2530–2539 (2023).
- ¹⁰W. Luo, B. J. Lawrie, A. A. Purezky, Q. Tan, H. Gao, D. B. Lingerfelt, G. Eichman, E. Mcgee, A. K. Swan, L. Liang, *et al.*, "Imaging strain-localized single-photon emitters in layered gas below the diffraction limit," *ACS nano* **17**, 23455–23465 (2023).
- ¹¹K. Parto, S. I. Azzam, K. Banerjee, and G. Moody, "Defect and strain engineering of monolayer wse₂ enables site-controlled single-photon emission up to 150 k," *Nature communications* **12**, 3585 (2021).
- ¹²O. Iff, D. Tedeschi, J. Martín-Sánchez, M. Moczala-Dusanowska, S. Tongay, K. Yumigeta, J. Taboada-Gutiérrez, M. Savaresi, A. Rastelli, P. Alonso-González, *et al.*, "Strain-tunable single photon sources in wse₂ monolayers," *Nano letters* **19**, 6931–6936 (2019).
- ¹³D. Curie, J. T. Kroegel, L. Cavar, A. Solanki, P. Upadhyaya, T. Li, Y.-Y. Pai, M. Chilcote, V. Iyer, A. Purezky, *et al.*, "Correlative nanoscale imaging of strained hbn spin defects," *ACS Applied Materials & Interfaces* **14**, 41361–41368 (2022).
- ¹⁴S. J. White, T. Yang, N. Dontschuk, C. Li, Z.-Q. Xu, M. Kianinia, A. Stacey, M. Toth, and I. Aharonovich, "Electrical control of quantum emitters in a van der waals heterostructure," *Light: Science & Applications* **11**, 186 (2022).
- ¹⁵W. Luo, A. Purezky, B. Lawrie, Q. Tan, H. Gao, A. K. Swan, L. Liang, and X. Ling, "Improving strain-localized gas single photon emitters with electrical doping," *Nano Letters* **23**, 9740–9747 (2023).
- ¹⁶K. G. Schadler, C. Ciancico, S. Pazzagli, P. Lombardi, A. Bachtold, C. Toninelli, A. Reserbat-Plantey, and F. H. Koppens, "Electrical control of lifetime-limited quantum emitters using 2d materials," *Nano letters* **19**, 3789–3795 (2019).
- ¹⁷M. A. Feldman, A. Purezky, L. Lindsay, E. Tucker, D. P. Briggs, P. G. Evans, R. F. Haglund, and B. J. Lawrie, "Phonon-induced multicolor correlations in hbn single-photon emitters," *Physical Review B* **99**, 020101 (2019).
- ¹⁸M. A. Feldman, C. E. Marvinney, A. A. Purezky, and B. J. Lawrie, "Evidence of photochromism in a hexagonal boron nitride single-photon emitter," *Optica* **8**, 1–5 (2020).
- ¹⁹N. Bonnet, J. Baaboura, F. Castioni, S. Y. Woo, C.-H. Ho, K. Watanabe, T. Taniguchi, L. H. Tizei, and T. Coenen, "Cathodoluminescence emission and electron energy loss absorption from a 2d transition metal dichalcogenide in van der waals heterostructures," *Nanotechnology* **35** (2024).
- ²⁰S. Roux, C. Fournier, K. Watanabe, T. Taniguchi, J.-P. Hermier, J. Barjon, and A. Delteil, "Cathodoluminescence monitoring of quantum emitter activation in hexagonal boron nitride," *Applied Physics Letters* **121** (2022).
- ²¹S. Zheng, J.-K. So, F. Liu, Z. Liu, N. Zheludev, and H. J. Fan, "Giant enhancement of cathodoluminescence of monolayer transitional metal dichalcogenides semiconductors," *Nano letters* **17**, 6475–6480 (2017).
- ²²S. Fiedler, S. Morozov, L. Iliushyn, S. Boroviks, M. Thomaschewski, J. Wang, T. J. Booth, N. Stenger, C. Wolff, and N. A. Mortensen, "Photon superbunching in cathodoluminescence of excitons in ws₂ monolayer," *2D Materials* **10** (2023).
- ²³V. Iyer, Y. S. Phang, A. Butler, J. Chen, B. Lerner, C. Argyropoulos, T. Hoang, and B. Lawrie, "Near-field imaging of plasmonic nanopatch antennas with integrated semiconductor quantum dots," *APL Photonics* **6** (2021).
- ²⁴J. Horder, S. J. White, A. Gale, C. Li, K. Watanabe, T. Taniguchi, M. Kianinia, I. Aharonovich, and M. Toth, "Coherence properties of electron-beam-activated emitters in hexagonal boron nitride under resonant excitation," *Physical Review Applied* **18**, 064021 (2022).
- ²⁵A. Gale, C. Li, Y. Chen, K. Watanabe, T. Taniguchi, I. Aharonovich, and M. Toth, "Site-specific fabrication of blue quantum emitters in hexagonal boron nitride," *ACS Photonics* **9**, 2170–2177 (2022).
- ²⁶F. Bianco, E. Corte, S. Ditalia Tchernij, J. Forneris, and F. Fabbri, "Engineering multicolor radiative centers in hbn flakes by varying the electron beam irradiation parameters," *Nanomaterials* **13**, 739 (2023).
- ²⁷F. D. Javan, F. Samadzadegan, S. Mehravar, A. Toosi, R. Khatami, and A. Stein, "A review of image fusion techniques for pan-sharpening of high-resolution satellite imagery," *ISPRS journal of photogrammetry and remote sensing* **171**, 101–117 (2021).
- ²⁸L. Loncan, L. B. De Almeida, J. M. Biucas-Dias, X. Briottet, J. Chanussot, N. Dobigeon, S. Fabre, W. Liao, G. A. Licciardi, M. Simoes, *et al.*, "Hyperspectral pansharpening: A review," *IEEE Geoscience and remote sensing magazine* **3**, 27–46 (2015).
- ²⁹N. Borodinov, P. Banerjee, S. C. Hum, D. J. Milliron, O. S. Ovchinnikova, R. K. Vasudevan, and J. A. Hachtel, "Enhancing hyperspectral cels analysis of complex plasmonic nanostructures with pan-sharpening," *Journal of Chemical Physics* **154**, 014202 (2021).
- ³⁰N. Borodinov, N. Bilkey, M. Foston, A. V. Ievlev, A. Belianinov, S. Jesse, R. K. Vasudevan, S. V. Kalinin, and O. S. Ovchinnikova, "Application of pan-sharpening algorithm for correlative multimodal imaging using afm-ir," *npj Computational Materials* **5** (2019).
- ³¹J. Tarolli, H. Tian, and N. Winograd, "Application of pan-sharpening to sims imaging," *Surface and Interface Analysis* **46**, 217–220 (2014).
- ³²G. Vivone, L. Alparone, J. Chanussot, M. Dalla Mura, A. Garzelli, G. A. Licciardi, R. Restaino, and L. Wald, "A critical comparison among pan-sharpening algorithms," *IEEE Transactions on Geoscience and Remote Sensing* **53**, 2565–2586 (2014).
- ³³A. R. Gillespie, A. B. Kahle, and R. E. Walker, "Color enhancement of highly correlated images. ii. channel ratio and "chromaticity" transformation techniques," *Remote Sensing of Environment* **22**, 343–365 (1987).